Jurnal Teknologi

Full Paper

INVESTIGATION ON CORROSION AND FLEXURAL BEHAVIOUR OF REINFORCED CONCRETE USING MARINE SAND

Karthikeyan Ganesan[a]*, Vijai Kanagarajan[b], Jerlin Regin Joseph Dominic[c]

[a]Department of Civil Engineering, Ramco Institute of Technology, Rajapalayam, Tamil Nadu, India
[b]Department of Civil Engineering, St. Joseph's College of Engineering, Chennai, Tamil Nadu, India
[c]Department of Civil Engineering, St. Xavier's Catholic College of Engineering, Nagercoil, Tamil Nadu, India

Article history
Received
25 February 2024
Received in revised form
13 June 2024
Accepted
16 July 2024
Published Online
22 December 2024

*Corresponding author
karthikeyang@ritrjpm.ac.in

Graphical abstract

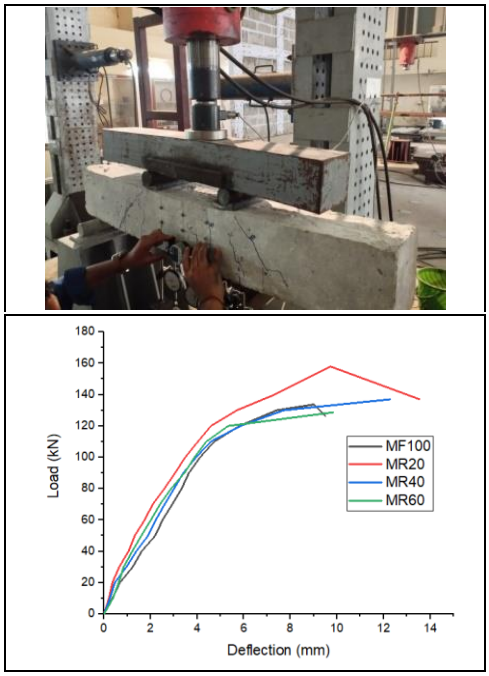

Abstract

Traditionally, the construction industry relies on both manufactured sand (known as MF-Sand) and river sand as primary constituents for fine aggregates. However, in response to the dwindling supply of river sand, the contemporary preference is firmly in favor of MF-Sand. This research focuses the utilization of meticulously cleaned marine sand (referred to as MR-Sand) as a superior substitute for MF-Sand, aiming to curtail the reliance on and depletion of river sand, a finite natural resource. The objective of this research is to examine the mechanical property of flexural performance of Reinforced Cement Concrete (RCC) Beam and durability study of concrete using corrosion test in which washed MR - Sand as a fine aggregate in partial replacement of MF-Sand from 20% to 60%. The physical and chemical characteristics of treated and untreated marine sand are compared with a view to better comprehending the features of MR and MF-Sand. Experimental research works have been carried out to look into the corrosion test and flexural strength in order to better understanding the strength and durability attributes of concrete. The values for flexural strength, ultimate load, load-deflection, load-strain, and crack pattern have been compared for the RCC beam specimens MF100, MR20, MR40 and MR60. The findings indicate that 60% of MR-Sand possesses the desired properties of strength and durability of concrete. Additionally, Finite Element Analysis is carried out using the ABAQUS software to further validate the experimental findings of load-deflection, load carrying capacity, crack pattern and flexural strength.

Keywords: Marine sand, concrete, corrosion, FEM and flexural strength

1.0 INTRODUCTION

After water, concrete is the second most commonly used material and serves as the foundation for urban development. It is estimated that ten billion tonnes of concrete are produced worldwide each year. Natural aggregate sources are becoming scarce in today's world, and their extraction has negative environmental effects. As a result, river sand consumption must be optimized, and alternative sources must be expanded to replace it. Globally, fine aggregate demand has skyrocketed because of the rapid expansion of construction projects, it has caused a shortage of natural fine aggregate (river sand). As a result, river sand must be replaced with another alternative in the production of concrete. The shortage of M-sand has made it more scarce and of high demand in the construction industry. Developing countries like India invest heavily in infrastructure as part of their plans to grow their economy. Examples of such activities include the construction of large structures, roads and railroads, and smart cities. Concrete is a necessary component of Indian construction and is required for many of these tasks. The widespread consumption of river sand is one of the main causes of its depletion, which is a major environmental concerns such as erosion and flooding. Hence, the flexural behaviour of RCC beam made with Marine Sand, durability studty and FEM analysis are investigated in this research work.

According to my previous study [1], sixty percent of the MR sample had higher compressive strength values than the control specimen MF100. This test demonstrates that the specimens using fine aggregates (MF100, MR20, MR40, and MR60) were able to achieve the required strength. It is suggested to use a mixture of 20% to 60% MR since it provides the required strength. High chloride concentrations in seawater and sea sand are anticipated to significantly accelerate the development of concrete strength in its early stages. Concrete made with marine sand has a significantly higher 7-day and long-term compressive strength than ordinary specimens [2]. Marine sand, which includes large quantities of chloride ions, can cause reinforcement in concrete to corrode, which in turn, affects the strength of the structure in the long-term. Marine sand needs to be washed before it is used in order to reduce the chloride ions present in it. Chloride ions in Marine Sand concrete make it more resistant to carbonization than desalted marine sand concrete [3] and [4].

From this investigation [18], stirrups and top reinforcements should be made of FRP, in addition to the tensile reinforcements, to prevent corrosion when utilising seawater and marine sand. In this research, SWSSC (sea water sea sand concret) beams fully reinforced with FRP bars underwent an accelerated ageing test in a maritime setting. Two varieties of beams underwent testing. Steel-FRP composite bars (SFCB) served as the tensile reinforcement in one, while basalt FRP (BFRP) bars served as the reinforcement in the other. The upper reinforcements and stirrups were made of BFRP bars. The experimental findings demonstrated that with exposure to the environment, cracks in both kinds of beams became scarce during bending testing.

In continue with my previous study [1], during the curing process, it has been noticed that, in mortars prepared using washed marine sand (WMR) and MR, the presence of free chloride content increases at first. After a while, it decreases and finally reaches stability. WMR and MR mortars tend to develop more porosity. This results in capillary holes that are smaller, with sizes between 10 and 100 nm [5]. The possibility of substituting MR for MF-Sand in concrete is examined in the current experimental and numerical study. In addition, it provides solution to the problem of excavating natural river sand.

2.0 METHODOLOGY

2.1 MF-Sand

In Figures 1 and 2 represents the MF-Sand (Manufactured Sand) and MR is visually depicted, illustrating various ratios employed in the quest to identify the optimal mixture. In this study, crushed aggregate from strong granite stone is employed as Manufactured Sand (MF-Sand) [9]. This aggregate has a cubic shape and comes with rounded edges.

It is washed thoroughly and graded uniformly. Figures 3 and 4 represents the XRD results of MF-Sand and Marine Sand respectively. It is carried out as per ASTM E1361. The sieve analysis as per IS 383 [10] and the PSD curve [11] shown in Figure 5 classify this aggregate under Zone II [24].

Figure 1 Manufactured Sand (MF-Sand)

Figure 2 Marine Sand (MR)

2.2 Marine Sand (MR)

For the current study, Marine Sand (MR) has been taken from the beach in Tiruchendur in Tamil Nadu. The same is represented in Figure 2. Marine Sand [7] was tested for physical properties (Table 1) as per IS: 2386-1963 [8], and IS: 383-1970 [9]. The PSD curve Figure 5 shows that, marine sand contains more amount of finer particles than the MF-Sand. It is an indication to get good binding property and closer matrix in the hardened state of concrete. Before and after washing, MR's chemical composition is examined using an XRD test to determine its chloride concentration. The chemical composition values are shown in Table 2 as per IS 14959 (Part 2) – 2001 [10]. In marine sand, chloride is present which, in turn, causes steel to corrode. In order to be used in concrete, it must be within the permitted limits (less than 0.05 percent). As a result, MR is dried and rinsed with fresh water to lower the Cl concentration to 0.02 percent (Table 2). Analysis of the particle size distribution curve unmistakably reveals that MS exhibits a finer granularity compared to M-Sand. Subsequently, the mix MR20 to MR60 can be classified under zone III, it represents slightly fine sand and the mix MR80 and MR100 can be classified under zone IV.

2.3 Removal of Chloride Contents

If there is too much chloride in concrete, it can cause corrosion in steel reinforcement and efflorescence because it has absorbed moisture from the air. Hence, the solubility of chloride content becomes a pivotal consideration when employing marine sand as a fine aggregate. The mechanical washing test with fresh water using concrete mixer was carried out to remove the chloride content and to investigate the suitability of marine sand for concrete production.

2.4 XRD Analysis of M-Sand and Marine Sand

XRD analysis is used to determine the crystalline phases present in MF-Sand and Marine Sand. It includes detailed information about the crystallographic structure and chemical compositions. The X-Ray diffraction analysis reveals prominent peaks at 27° angles for both MF-Sand and Marine Sand, underscoring the prevalence of silica as the primary constituent in all four samples. It indicates that the available silica was crystalline in nature.

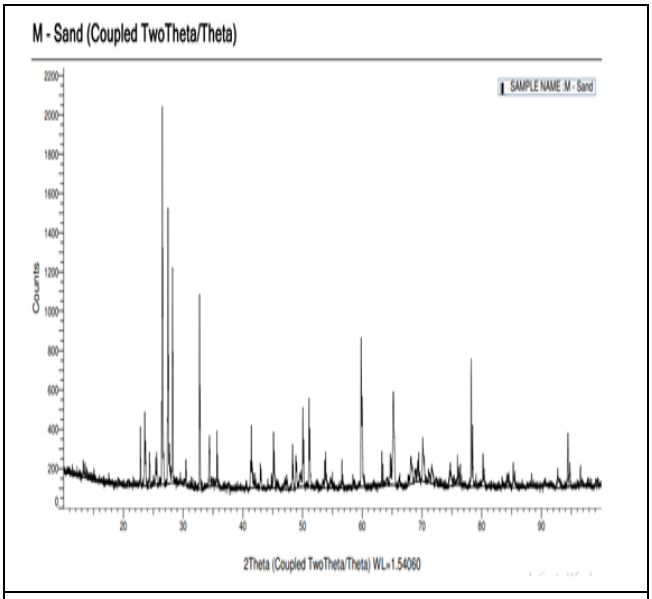

Figure 3 XRD Analysis of MF-Sand

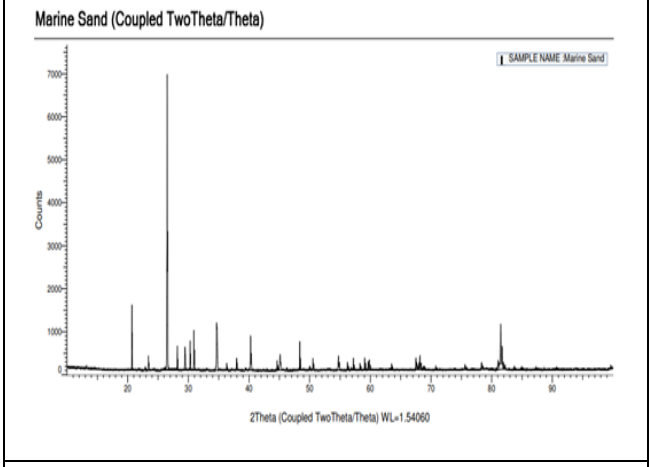

Figure 4 XRD Analysis of Marine Sand (MR)

Table 1 Fine and Coarse Aggregates' Characteristics

Physical Property	MF-Sand	Marine Sand (MR)	Coarse Aggregate
Specific gravity	2.65	2.65	2.7
Fineness modulus	3.48	2.26	7.4
Bulk Density in kg/m^3	1596	1287	1650
Water absorption	2.56%	1.93%	0.6%

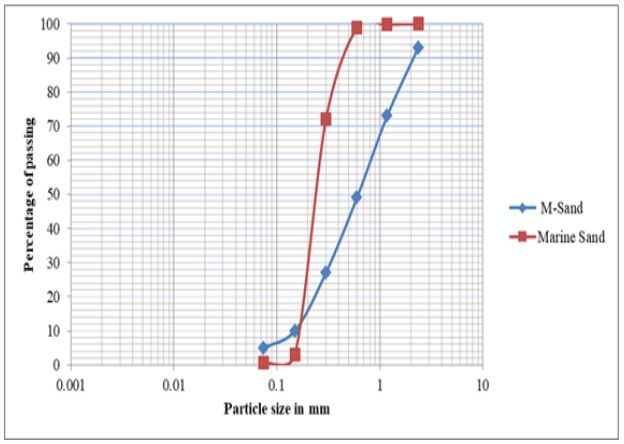

Figure 5 PSD Curve

2.5 Cement

Conforming to IS: 12269-2013, this study employs Ordinary Portland Cement of the 53-grade [11] was taken from Virudhunagar and tested for its consistency, fineness and soundness as per IS 4031:1988 [25]. In a similar manner, the determination of the cement's specific gravity was conducted in accordance with IS 2720-1980. The results revealed that it has a specific gravity of 3.12 and soundness of 4.6 mm.

2.6 Coarse Aggregate (CA) and Reinforcement

It exhibits a specific gravity of 2.7 and a fineness modulus of 7.4, bulk density of 1650 kg/m^3 and a dry density of 2550 kg/m^3 with a grading zone of II and 0.6 percent water absorption. The above properties are tested as per IS: 2386-1963 [12]. Refer Table 1 for the physical characteristics of aggregates which is used for the various mixes. 12mm, 10mm and 8 mm HYSD bars are used for longitudinal reinforcement [13] for bottom, top and lateral ties respectively.

Table 2 Chemical Composition of Marine Sand (MR)

Properties	Si	O	Ca	K	Fe	Cl
Before washing	30.21%	43.39%	15.36%	8.58%	2.46%	0.05%
Washed and dried	43.40 %	51.01%	5.59%	-	-	0.02%

2.7 M25 Grade's Mix Design

The mix proportion is arrived (Table 3) according to IS 456:2000 [14] and IS 10262:2009 [15] for concrete mix design of M25 grade. The mixing ratio is set at 1:1.69:2.93, accompanied by a water content of 197 kg/m^3.

Table 3 Quantity in kg/m^3

Mix ID	Cement	Water	M-Sand	MS	CA
MF100	419.15	197	709	-	1230

2.8 Test Methods for Concrete

The following mechanical characteristics of concrete (Figure 6) are examined in accordance with IS 516-1959 [16] & IS 456:2000 [14]. In addition, to further validate the experimental findings, Finite Element Analysis (FEA) simulations of RCC beams were conducted using the ABAQUS software.

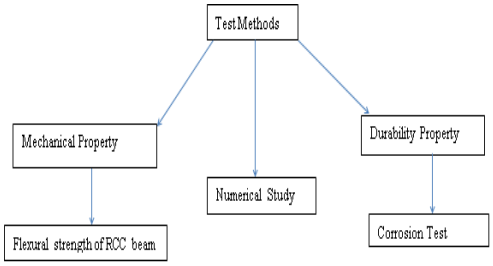

Figure 6 Test Methods

2.9 Flexural Strength of RCC Beam

Reinforced concrete beams measuring 150 mm x 200 mm x 1200 mm were cast to determine flexural strength on a large scale. During fabrication, precautions were taken to prevent localized buckling. There was also a clear cover of 25 mm provided to the reinforcement. Reinforced Cement Concrete beam was designed as per IS: 456-2000 [14] for a span of 1200 mm. In accordance with the structural design, the bottom of the beam was reinforced with two 12 mm diameter bars, while the top was fortified with two 10 mm diameter bars. In accordance with IS 5525 – 1969, shear reinforcement was provided throughout the span as 8mm bars at 100 mm c/c. MF100, MR20, MR40, and MR60 beams were cast based on the mechanical property results. To ensure proper compaction, needle vibrator has been used. Beam dimension, fabrication and reinforcement details for RCC beam as shown in Figures 7 and 8. RCC beam of 150 mm x 200 mm x 1200 mm was tested under bending conditions as per Figure 13. The flexural strength [18] of four specimens such as MF100, MR20, MR40 and MR60 was calculated using loading frame and the equation 3.1 is given below. Casting of RCC beam is shown in Figure 9. Testing was done as per IS 516-1959 [16].

$$\text{Flexural Strength } fb = PL/bd^2 \quad (3.1)$$

Where, b = Width (mm), d = Depth (mm)
L = Length (mm) and P = Ultimate load (N)

Figure 10 illustrate the curing process for the RCC beam. For the application of loads, a hydraulic jack with a 500 kN capacity was employed, while deflection measurements were obtained using dial gauges placed at the beam's lower section. The load increment was done at an interval of 10 kN. At each load interval, deflection measurements and strain measurements were performed. The load at which the first crack developed has been observed and

corresponding deflections were noted down. This procedure was repeated for all the beams, the maximum load and corresponding deflection for each beam were recorded. For measuring the strains, nine demountable mechanical (DEMEC) points along the depth of the beam were located by attaching pellets on the beam. These pellets were positioned apart at 100 mm from each other to take strain measurements between pellets. From these readings, the strain of the beam was calculated. The load was transferred through the RS Joist beam. To record the deflection, three dial gauges were installed under the loading point system. Figure 17 shows measuring deflection and strain in the RCC beam.

The load-deformation behaviour of RCC beams of M100, MS20, MS40 and MS60 were studied for pure bending by subjecting it to a four point bending test. The following key structural parameters were observed, including the first cracking load (Pcr), yield load (Py), and ultimate load (Pu). The load – displacement behaviour exhibited by the specimens under bending and the load - strain graph for the beams MF100, MR20, MR40 and MR60 have been plotted. Table 4 displays the RCC beam's flexural strength and the same has been plotted [14].

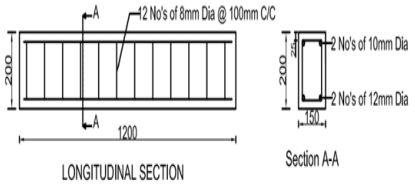

Figure 7 Dimension details for RCC beam

Figure 8 Preparation of Beam Reinforcement

Figure 9 Casting of RCC Beam

Figure 10 Curing of RCC beam

2.10 Corrosion Test

Despite the fact that concrete is a corrosion-resistant material, corrosion testing became necessary as washed marine sand was used as a substitute fine aggregate. Normally, chloride attack causes concrete to deteriorate, followed by reinforcement corrosion. The corrosion of concrete reinforcements has a greater impact on the structure's durability and serviceability. The tensile strength of reinforcement, as well as the adhesion between steel and concrete, decreases as the cross-sectional area decreases. A steel bar of 12 mm diameter was embedded in each of the 100 mm in diameter and 50 mm in height cylinder specimens to study the corrosion of concrete. After curing the samples for 28 days, they were subjected to alternate wetting and drying operations in accordance with ASTM C876 [20] as shown in Figure 11 and Figure 12. The specimens were dipped in a 3 percent NaCl solution during the wetting cycle for 15 days and then dried for 15 days (Figure 14). Before starting impressed voltage, the procedure was repeated twice. The specimens were pre-treated to speed up the corrosion process. Following the pretreatment, specimens were put through an impressed voltage test, which involved impressing 12V between a rebar anode and a stainless steel cathode in a 5% NaCl solution [24].

Figure 11 depicts the specimen details for corrosion test; figure 12 depicts the schematic diagram; Figure 13 depicts the casting; Figure 14 shows the curing of specimen for corrosion test. For each system, the time it took for an initial crack was recorded. After the specimens corroded, the weight loss due to rebar corrosion was calculated, as well as the corrosion rate of the mixes. Using the Equation (3.2), the corrosion rate was calculated.

$$\text{CorrosionRate(mmpy)} = \frac{(\text{Weight Loss} \times 87.60)}{6.8 \times (\text{Area} \times \text{Time} \times \text{Metal Density})} \quad (3.2)$$

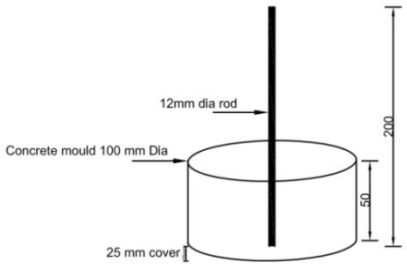

Figure 11 Specimen details for corrosion test

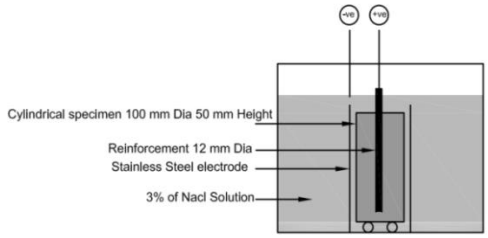

Figure 12 Schematic diagram of impressed voltage test

Figure 13 Casting of specimen for corrosion test

Figure 14 Curing of specimen for corrosion test

3.0 RESULTS AND DISCUSSION

The mechanical properties [17] of flexural strength of RCC beams are examined in accordance with IS 516-1959 [16] and the durability properties of corrosion test are assessed using impressed voltage test.

3.1 Flexural Strength of RCC Beam

Figures 15 and 16 shows that flexure test set up of RCC beam and RCC beam configuration respectively.Table 4 displays the RCC beam's flexural strength. Figures 17 and 18 shows that the measuring deflecton of RCC beam and flexural strength respectively.

Table 4 RCC Beam's Flexural Strength

No.	Mix ID	Flexural Strength (N/mm²) for 28 Days
1	MF100	22.28
2	MR20	26.33
3	MR40	22.83
4	MR60	21.45

It is noticed that the maximum flexural strength for the RCC beam MR20 is 26.33 N/mm² which is 18.2 % more than the control beam MF100.For the MR40, the maximum flexural strength is 22.83 N/mm² which is 2.5 % greater than the control specimen. It is due to the flexural performance and its high load carrying capacity. This is because Marine Sand was used as an aggregate, which inhibits the expansion of cracks in the cement paste by requiring more energy to break down and thereby stopping the fracture from getting wider.When compared to the control beam M100, the flexural strength of MS60 decreases to 3.7% as a result of the higher marine sand replacement percentage. Notably, the flexural strength of RCC beams with MR20, MR40, and MR60 is nearly equivalent to that of the control beam MF100.

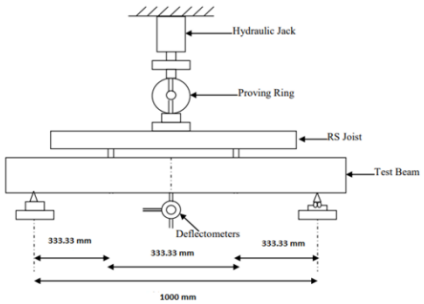

Figure 15 Flexure Test Set up

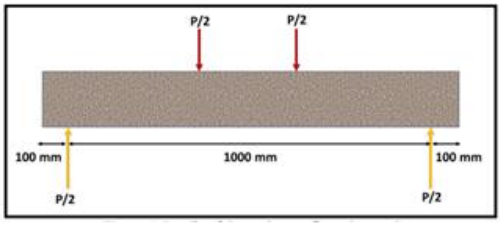

Figure 16 Flexure Testing of RCC Beam Configuration

Figure 17 Measuring deflection and strain in the RCC beam

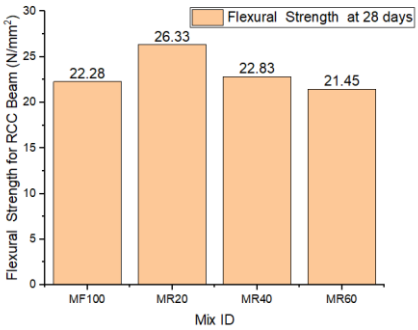

Figure 18 Flexural Strength of RCC Beam

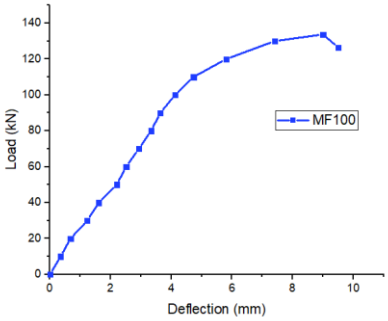

Figure 19a Load Vs Mid Span Deflection for MF100

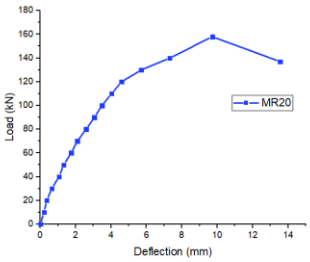

Figure 19b Load Vs Mid Span Deflection for MR20

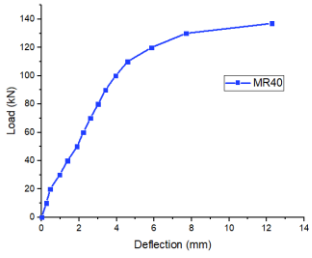

Figure 19c Load Vs Mid Span Deflection for MR40

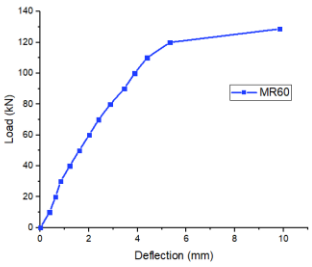

Figure 19d Load Vs Mid Span Deflection for MR60

While analysing the load carrying capacity and the lowest maximum deflection (3.22 mm), it yielded the best results in terms of flexural performance. This is largely because of the macro fibres present in it [23]. The beam MF100 exhibits an initial cracking load of 50 kN, with a corresponding mid-span deflection measuring 2.2 mm. Furthermore, the conventional beam MF100 demonstrates a maximum load-carrying capacity of 133.7 kN, accompanied by a peak deflection of 9.5 mm.

Figures 19 (a), (b), (c) and (d) illustrate the load vs mid span deflection for RCC beam MF100, MR20, MR40, MR60 respectively. At the onset of cracking in the MR20 beam, a load of 40 kN is observed, along with a deflection of 1.05 mm. The beam reaches its maximum load-carrying capacity at 158 kN, concurrently exhibiting a peak deflection of 13.55 mm. Similarly, a load of 40 kN and a deformation of 1.38 mm are noticed at the first crack of the beam MR40, where the maximum load carrying capacity is 137 kN and the maximum deformation is 12.28 mm. The load at first crack for the beam MR60 is 35 kN and the deformation is 1.12 mm. The maximum load carrying capacity for the beam is 128.7 kN and the maximum deformation is 9.85 mm for the beam MR60.

Figure 20 depicts the load-mid-span deflection relationships for each of the beams, including MF100, MR20, MR40, and MR60. The load vs strain (tensile and compressive) values for all the beams are plotted as shown in Figures 21 and 22. Figures 23 (a), (b), (c), and (d) illustrate the crack patterns observed in beams MF100, MR20, MR40, and MR60, respectively. The ultimate load, deflection, stiffness and ductility parameters are given in Table 5. The load vs midspan deflection behaviour of control specimen MF100 and the partial replacement made with MR beams MR20, MR40 and MR60 are almost similar due to the finer particles of MR.

From the load–tensile strain behaviour as per Figure 21, all the mixes MF100, MR20, MR40 and MR60 are similar. For the given loading, compared to MF100, MR20 specimens have undergone more strain due to the partial replacement of marine sand.

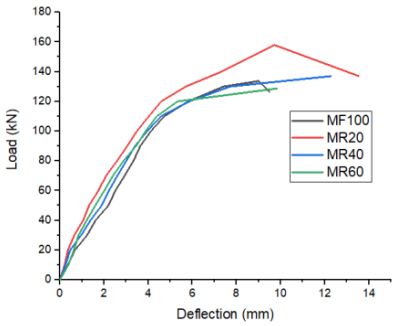

Figure 20 Load Vs Mid Span Deflection

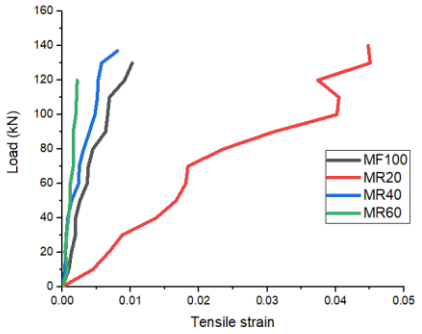

Figure 21 Load Vs Strain (Tensile)

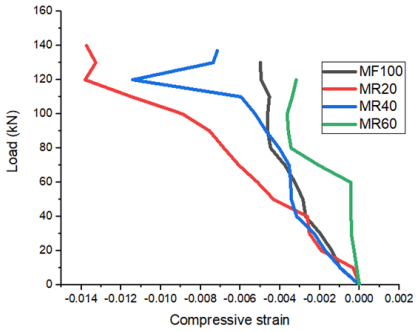

Figure 22 Load Vs Strain (Compressive)

From the load–compressive strain behaviour as per Figure 22, all the mixes MF100, MR20, MR40 and MR60 are similar. Under the applied load conditions, the MR40 specimen experiences greater strain in comparison to MF100, owing to the partial substitution of marine sand.

Figure 23a Crack Formation in the MF100 Beam

Figure 23b Crack Formation in the MR20 Beam

Figure 23c Crack Formation in the MR40 Beam

Figure 23d Crack Formation in the MR60 Beam

Table 5 Ultimate load, Deflection, Stiffness and Ductility

Mix Id	Load (kN)		Deflection (mm)		Initial stiffness (kN/mm)	Ultimate stiffness (kN/mm)	Energy ductility Index (Pu/Px)	Displacement ductility index(Δu/Δx)
	Yield Px	Ultimate Pu	Yield Δx	Ultimate Δu				
MF100	120	133.7	5.81	9	20.65	14.86	1.11	1.55
MR20	128	158	5.68	9.72	22.54	16.26	1.23	1.71
MR40	110	137	4.58	12.28	24.02	11.16	1.25	2.68
MR60	120	128.7	5.33	9.85	22.51	13.07	1.07	1.85

The beam MF100 is subjected to an ultimate load of133.7 kN and the initial stiffness and ultimate stiffness values are 20.65 kN/mm and 14.86 kN/mm respectively. The specimen MR20 has a stiffness of 16.26 kN/mm. It is 9.4% higher than that of MF100. The marine sand-based beams MR20 and MR60 were found to have greater stiffness and less deflection. From the above comparison of results, the maximum load carrying capacity which is 158 kN, together with a minimum deflection of 9.72 mm occurs due to the presence of finer particle of marine sand and the bonding of cement matrix [1]. The deflection, initial stiffness, energy ductility index, displacement ductility index for the beam MR20,

MR40, MR60 are similar to the conventional beam MF100 due to the mixture of fine particles of M-Sand and marine sand and the beam's flexural capability. The deflection for the beam MR40 is 36.4% higher than the conventional beam MF100 and the deflection for the beam MR60 is 9.44% higher than the conventional beam MF100 due to the partial replacement of fine aggregate.

3.2 First Crack and Load – Deflection Behaviour for RCC Beam

In the preceding examination of load-deflection behavior, a noticeable delay is noted in the initiation of the initial crack formation. The displacement and number of cracks are within the limits for all mixes. The beam MF100 exhibits its initial crack, measuring 24 mm in length, at a load of 50 kN. Conversely, the beam MS20 experiences its first crack, measuring 31 mm, under a 40 kN load. Meanwhile, the beam MS60 displays its first crack, spanning 25 mm, when subjected to a load of 35 kN. All observed cracks are minor and originate from the tension zone of the beam. The load-deflection behaviours of MR20 and MR60 were found to be similar to the control beam M100. Maximum deflection has been noticed in the case of M100 while the corresponding load being 133.7 kN. While comparing control mixes for beam M100, MS20, MS60, good load-deflection behaviour is noticeable. Beam MS20 has the maximum load carrying capacity of 158 kN. The values for initial stiffness, ultimate stiffness, and energy ductility index for the beams MR20, MR40, and MR60 were found to be similar to those for the control beam MF100. Analysis of the existing literature confirms an 8.45% increase in flexural strength for the replaced beam in comparison to the conventional beam, and it also reveals that the load-deformation curve remains nearly identical across all the beams [3]. This is due to the addition of MS as an aggregate, which acts as a barrier to crack expansion in the cement paste.

3.3 Load – Strain Behaviour of RCC beam

The load–strain behaviour of RCC beam control specimens MF100 and MR20, MR40 and MR60 are almost similar. The flexural (bending) strength of RCC beam MF100 is 22.28 N/mm^2. The beam MR20 showcases a remarkable 18.18% increase in its bending strength when compared to the conventional MF100 beam. Meanwhile, the beam MR40 displays a modest 2.47% improvement in bending strength over the conventional MF100 beam. As a result of the marine sand partial replacement, the MR20 beam exhibited the most substantial load-bearing capacity with regards to its flexural performance. All of the beams MF100, MR20, MR40, and MR60 have similar crack patterns.

From the existing results [19] the stress – strain behaviour of beam MF100 and MR100 are almost same. D40 specimen has more strain compared to that of the control specimen.

3.4 Durability Properties of Concrete for Corrosion Test Using Impressed Voltage Test

Figure 24 depicts the corrosion test setup. After the specimens corroded (Figure 25), the weight loss due to rebar corrosion was calculated. The corrosion rates for all the percentages of replacements were determined using the equation (3.1) and the results are compared in Figure 26. Figure 27 compares the time taken for crack formation. This experiment was done with respect to the crack period of control concrete. A crack was noticed in marine sand replacement of 80% and 100% before control concrete. The experiment was continued till crack formation was observed, which eventually happened on the 15th day of the testing. Other specimens did not register any crack until then. Moreover, MR specimens of up to 60% are observed to be preventive in the external environment. Hence, these specimens had better resistance towards the external environment and performed well. The corrosion rates for all the specimens were found to be similar to the control concrete MF100, except specimens MR80 and MR100.

Figure 24 Corrosion Test Setup

Figure 25 Test specimen after corrosion

As per Table 6, the corrosion rate was higher in the 100% Marine sand replacement specimen (i.e) 3.4122 mmpy. Corrosion rates were higher for all the specimens other than 20% replacement compared with control concrete. The replacement of marine sand by 20 to 60% reduced current consumption and demonstrated good chloride diffuseability through low permeability, resulting in higher durability.

Table 6 Corrosion Rate

No.	Mix ID	Corrosion Rate (mmpy)
1	MF100	0.1133
2	MR20	0.1672
3	MR40	0.3826
4	MR60	1.1233
5	MR80	1.8971
6	MR100	3.4122

Figure 27 shows the current in corroded specimen and the percentage of replacement. From the results, it is clear that 80% and 100% of marine sand consumed more current, which indicates its higher corrosion rate. 20% to 60% of replacements of marine sand consumed lesser current than the control specimen, which proves its better durability characteristics.

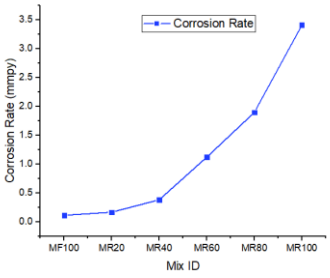

Figure 26 Corrosion Rate

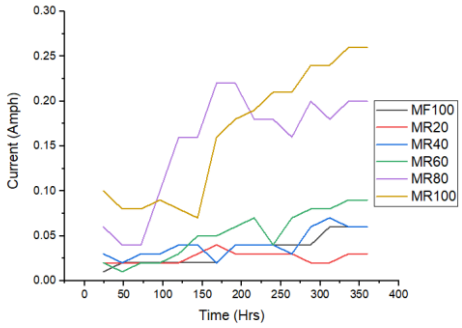

Figure 27 Current Vs Percentage of replacement

3.5 Numerical Study

A beam with dimensions of 150 x 200 x 1200 mm was used in this analytical work as shown in figure 28 (a). In the part module, the RCC beam, the longitudinal reinforcement, the transverse reinforcement, and meshes have all been created separately. In the part module, the beam is indicated by selecting 3D solid as a modelling space and deformable as a type. The beam part is made by drawing the beam's geometry and extruding it. For the application of load and boundary conditions, the partition command is used. According to the IS code, the beam cover is 25mm. Figures 28(a) and (b) show the developed RCC beam model as well as the assembled part. Figure 28(c) and (d) represent the loading part and the mesh creation, respectively.

Young's modulus and Poisson's ratio play a pivotal role in delineating the elastic characteristics of concrete. The Concrete Damaged Plasticity Model (CDP) is employed for characterizing the plastic behavior of concrete. This versatile model finds application in a broad spectrum of structures, allowing for the representation of the inelastic properties of concrete by integrating principles of isotropic damaged elasticity with both tensile and compressive plasticity. Incorporated within the property module, this non-linear analysis encompasses the specification of both elastic and plastic material attributes. For M25 grade beams, Young's modulus is set at 25,000 N/mm^2, while the Poisson's ratio is established at 0.2. The damage properties for both tension and compression have been included in this step. The reinforcement used top rebar diameters of 10 mm, bottom rebar diameters of 12 mm, and stirrup diameters of 8 mm @ 100 mm. In loading part, the reinforced beam has pinned support at both ends. Vertical loading is applied at the midpoint of the reinforced beam. The load value is taken from the experimental test.

3.6 Finite Element Analysis Results & Discussion

The fine element modeling of RCC beams MF100, MR20, MR40 and MR60 of mesh was done using ABAQUS [22] and the results in terms of deflection, stress contours, compression damage, and tension damage of each type of beam are determined and compared. The beam was subjected to finite element analysis.

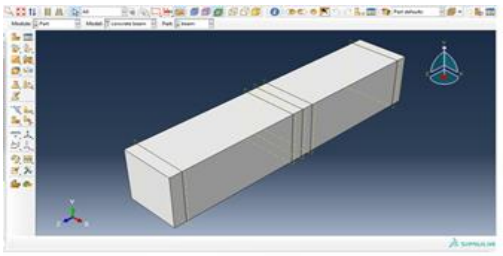

Figure 28a RCC Beam Modeling

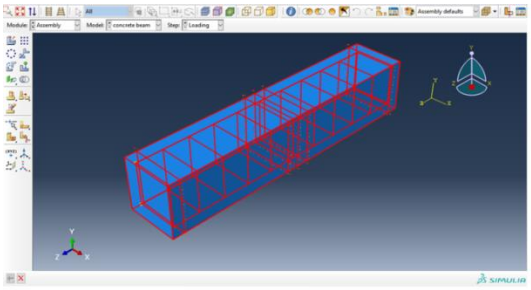

Figure 28b Assemble part

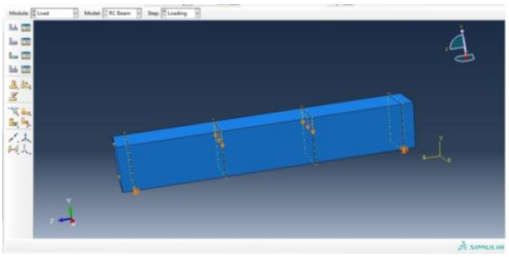

Figure 28c Loading part

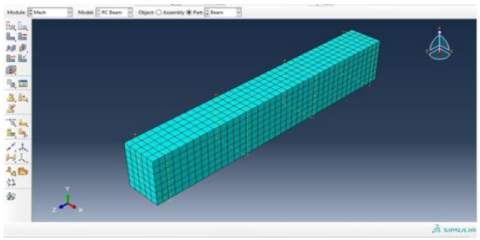

Figure 28d Mesh Creation

The specimen results that were subjected to maximum load have been obtained and the deflection in the experimental work has been validated. The maximum deflection of experimental and analytical results has been tabulated at the end of the chapter for validation.

3.7 Deflection of RCC Beam under Flexure

Figures 29(a), (b), (c), and (d) depict the deformed states of beams MF100, MR20, MR40, and MR60, revealing maximum deflections at the center measuring 9.25 mm, 9.44 mm, 9.83 mm, and 10.21 mm, respectively.

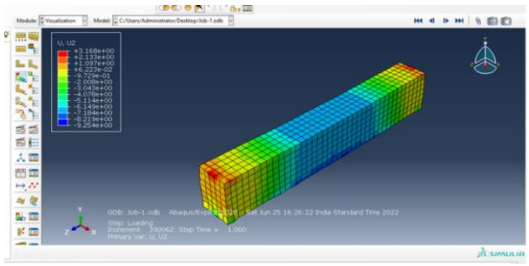

Figure 29a Deformation of RCC beam MF100

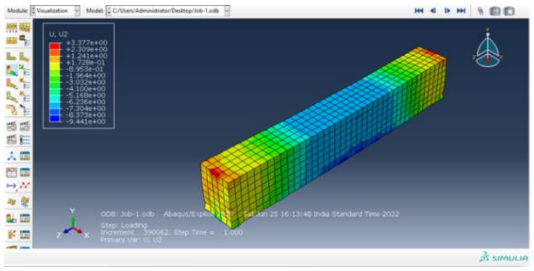

Figure 29b Deformation of RCC beam MR20

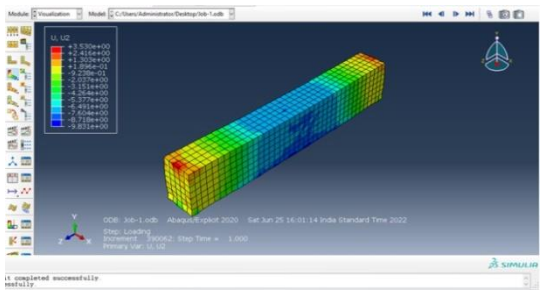

Figure 29c Deformation of RCC beam MR40

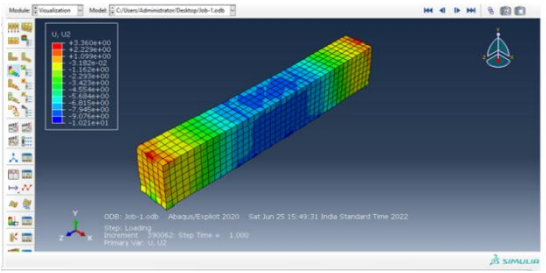

Figure 29d Deformation of RCC beam MR60

The deflection for the RCC beam with 20%, 40%, and 60% replacements of Marine Sand samples increased by 2.05%, 6.27%, and 10.38% respectively, in comparison to control beam M100. This is largely because of the increase in deflection at mid span. From the flexural behaviour, it is clear that MR20 beam has the maximum load carrying capacity; however, it has a lower deflection because of the presence of marine sand. Damage is distributed in layers because of the distribution of the stress in the concrete element.

3.8 Stress Contour of RCC Beam under Flexure

Figures 30 (a), (b), (c) and (d) show the stress contour of beams MF100, MR20, MR40 and MR60 respectively. From the results, it is noticed that the major stresses are induced due to bending and the stress contour shows that the maximum stress occurs at the top of compressive fibre of the beam. The MR20, MR40, and MR60 beams also experience a similar type of compressive stress. According to the existing results [23] the flexural strength for the specimens SP 5 and SP 6 is 5.367 N/mm^2 and 5.167 N/mm^2 respectively. This marks an increase of 42.22% and 47.73% in comparison to the conventional mix's strength (3.633 MPa). The introduction of macro and microfibers contributes to reduced deflection by facilitating a bridging effect.

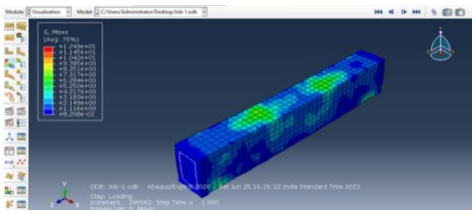

Figure 30a Stress contour for RCC beam MF100

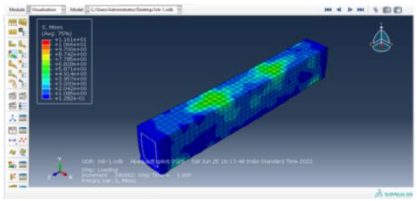

Figure 30b Stress contour for RCC beam MR20

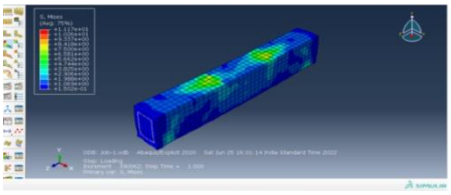

Figure 30c Stress contour for RCC beam MR40

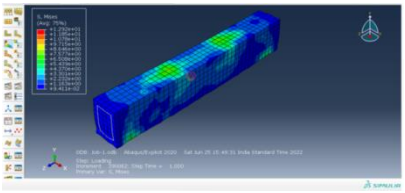

Figure 30d Stress contour for RCC beam MR60

3.9 Compression and Tension Damage

From the results, the compression damage and tension damage have been induced due to bending, and the failure of the beam occurs at the top of the compressive fibre due to the maximum stress induced and at the tensile fibre of the beam due to the maximum deflection. The same type of failure occurs for the beams MR20,MR40 and MR60 when compared to conventional beam M100 while subjected to the RCC beam flexure test. Similar compression and tension damage occurs to beams MR20, MR40, and MR60 as it does to the standard beam MF100.

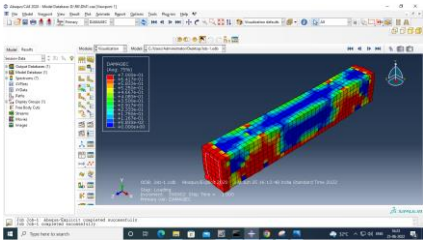

Figure 31 Compression damage for beam MR20

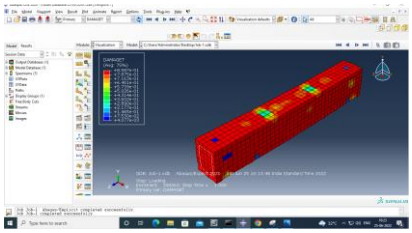

Figure 32 Tension damage for beam MR20

The flexural behaviour of RCC beam has been investigated experimentally using two point bending test to study the load-deflection, load-strain, maximum load carrying capacity, crack patter and flexural strength. To validate the above experimental results, Finite Element Method is used for modeling the RCC beam and analyzing the flexural behaviour for maximum deflection, stress contour, compression damage and tension damage, which are found to be almost similar. From the above results, it is clear that the compression damage for beam MR20 is almost the same as that of the control beam MF100. In RCC beam, the flexural cracks occur when it exceeds the load carrying capacity of the beam. The compression and tension damage behaviour for beam MR20 is shown in Figure 31 and 32. From the above results, the compression damage for beam MR60 is almost the same as that of control beam MF100. Flexural cracks occur in RCC beam when the load carrying capacity is exceeded. The above results reveal that the tension damage of beam MR60 is almost the same as that of the control beam MF100. The comparison of experimental and analytical results is presented in Table 7 and Figure 33.

From the above comparison, the maximum deflection for the RCC beams MR20, MR40, MR60 are similar to that of conventional RCC beam M100. The maximum variation for deflection of beam using analytical and experimental work is 2.45 for the beam MR40.

Table 7 Comparison of Beam deflection results

No.	Mix ID	Maximum Deflection (mm)	Variation	Analytical Experimental
1.	MF100	9.25	9	0.25
2.	MR20	9.44	9.72	0.28
3.	MS40	9.83	12.28	2.45
4.	MS60	10.21	9.85	0.36

From the experimental test, the maximum deflection for the beam MR40 is 12.28 mm which is 36% more than conventional beam MF100. This is because of the bonding of the ITZ in concrete and replacing the marine sand partially. From the analytical study, the maximum deflection for the RCC beam MR60 is 10.21 mm which is 10.3% more than conventional beam MF100. The variations for maximum deflection of beam between the

analytical and experimental results are minimum. From the above comparison, the results are validated for the deflection of beam at mid span. From the above comparison, it is clear that the bending behaviour of RCC beam made with marine sand is almost similar to the control beam.

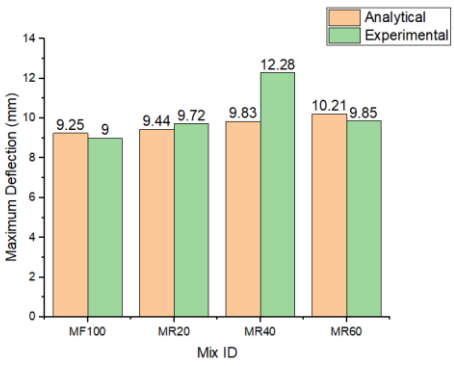

Figure 33 Comparison of Beam Deflection

4.0 CONCLUSION

The outcomes of both the experimental and numerical investigations are as follows:

Based on the experimental results of flexural behaviour of RCC beams MR20, MR40, MR60 values of flexural strength, maximum deflection,crack pattern, load vs deflection and load vs strain values are similar tothat conventional beam MF100.The numerical study for the beam was investigated using ABAQUS FEM model and the results have been validated to be similar to that of experimental results. 20% of Marine Sand replacement in beams showed higher ultimate strength than the control beam. The beam of MR60 provided the same strength as that of the control beam. The 20% to 60% replacements of marine sand consumed less current. It also demonstrated good chloride permeability by exhibiting low permeability, which results in better durability characteristics. According to the results of the aforementioned experimental and numerical studies, it is suggested to substitute 60% of MF-Sand by washed marine sand (MR) in construction applications like brickwork, plain cement concrete, pavements, plastering and other structural works.

Acknowledgement

The authors are indebted to the Management and the Principal of Ramco Institute of Technology, Rajapalayam, Tamil Nadu, India for providing necessary facilities to carry out this research work.

Conflicts of Interest

The author(s) declare(s) that there is no conflict of interest regarding the publication of this paper.

References

[1] Ganesan, K., Kanagarajan, V., & Dominic, J. R. J. 2022. Influence of Marine Sand as Fine Aggregate on Mechanical and Durability Properties of Cement Mortar and Concrete. *Materials Research Express*. 9(3).
[2] Xiao, J., Qiang, C., Nanni, A., & Zhang, K. 2017. Use of Sea-sand and Seawater in Concrete Construction: Current Status and Future Opportunities. *Construction and Building Materials*. 155: 1101-1111.
[3] Franchis David, M., Theenathayalan, R., Naganathaprabhu, L., & Vincent, P. 2019. Flexural Behavior of Sustainable Self-Compacting Concrete Beam. *Journal of Green Engineering*. 9(2): 176.
[4] Balaji, G., & Vetturayasudharsanan, R. 2020. Experimental Investigation on Flexural Behaviour of RC Hollow Beams. *Materials Today: Proceedings*. 21(July): 351.
[5] Sun, C., Sun, M., Tao, T., Qu, F., Wang, G., Zhang, P., … Duan, J. 2021. Chloride Binding Capacity and Its Effect on the Microstructure of Mortar Made with Marine Sand. *Sustainability (Switzerland)*. 13(8).
[6] Regin, J. Jerlin Regin, J., Vincent, P. & Ganapathy, C. 2014. An Experimental Study on Partial Replacement of Cement by Silica Fume and Fly Ash in Lightweight Coconut Shell Concrete (April 2014). *International Journal of Earth Sciences and Engineering*. 7(5): 980-986.
[7] Liu, W., Huang, R., Fu, J., Tang, W., Dong, Z., & Cui, H. 2018. Discussion and Experiments on the Limits of Chloride, Sulphate and Shell Content in Marine Fine Aggregates for Concrete. *Construction and Building Materials*. 159: 725.
[8] IS:2386- PART I. 1963. Method of Test for Aggregate for Concrete. Part I - Particle Size and Shape. Indian Standards, (Reaffirmed 2002).
[9] IS:383. 1970. Specification for Coarse and Fine Aggregates from Natural Sources for Concrete. Indian Standards (Vol. 383).
[10] Bhavan, M. 2021. Determination of Water Soluble and Acid Soluble Chlorides in Mortar Concrete — M Ethod of Test. Bureau of Indian Standards (BIS) (Vol. 14959).
[11] IS 12269. 2013. IS (Indian Standard). 2013. Ordinary Portland Cement, 53 Grade — Specification. IS 12269-13. Bureau of Indian Standards. 6(2): 141.
[12] IS 2386- PART III. 1963. Method of Test for Aggregate for Concrete. Part III- Specific Gravity, Density, Voids, Absorption and Bulking. Bureau of Indian Standards, New Delhi, (Reaffirmed 2002).
[13] M. Karankumar, S. Sujith, & G. Karthikeyan. 2018. Structural Rehabilitation and Strengthening of Column using Micro Concrete and Additional Reinforcement. *International Journal of Engineering Research & Technology (IJERT)*. 7(06): 1.
[14] IS 456. 2000. Plain Concrete and Reinforced. Bureau of Indian Standards, New Dehli.
[15] IS:10262 - 2009. Guidelines for Concrete Mix Design Proportioning. Bureau of Indian Standards, New Delhi.
[16] IS 516. 1959. Method of Tests for Strength of Concrete. Bureau of Indian Standards.
[17] Jerlin Regin, J., Vincent, P., & Ganapathy, C. 2017. Effect of Mineral Admixtures on Mechanical Properties and Chemical Resistance of Lightweight Coconut Shell Concrete. *Arabian Journal for Science and Engineering*. 42(3): 957.
[18] Dong, Z., Wu, G., Zhao, X. L., Zhu, H., & Lian, J. L. 2018. Durability Test on the Flexural Performance of Seawater Sea-sand Concrete Beams Completely Reinforced with FRP Bars. *Construction and Building Materials*. 192: 671.

[19] Anbarasan, I., & Soundarapandian, N. 2020. Investigation of Mechanical and Micro Structural Properties of Geopolymer Concrete Blended by Dredged Marine Sand and Manufactured Sand under Ambient Curing Conditions. *Structural Concrete*. 21(3): 992.
[20] ASTM International. 2015. Standard Test Method for Corrosion Potentials of Uncoated Reinforcing Steel in Concrete. ASTM C876 - 15. G01.14. ASTM International. 1.
[21] Feng, B., Liu, J., Wei, J., Zhang, Y., Chen, Y., Wang, Sun, Z. 2021. Research on Properties and Durability of Desalinated Sea Sand Cement Modified with Fly Ash. *Case Studies in Construction Materials.* 15.
[22] Sakkarai, D., & Soundarapandian, N. 2021. Strength Behavior of Flat and Folded Fly Ash-based Geopolymer Ferrocement Panels under Flexure and Impact. *Advances in Civil Engineering.*
[23] Subramanian, J. S., Haamidh, A., & Krishiga, K. 2022. Assessment of Hybrid FRC Composite with Emphasis on the Flexural Performance of Functionally Graded Concrete. *AIP Conference Proceedings.* 2463(May).
[24] Ghutham, J., Bhuvanaeshwari, M., & Rooby, J. 2016. Experimental Study on Mechanical Properties of Rub-fibre Reinforced Concrete. *International Journal of Chemical Sciences.* 14: 65.
[25] Karthikeyan, G., Dharmar, S., Ragavan, V., Harshani, R. 2023. Study on Performance of Paver Block using Prosopis Juliflora Ash. *Global Nest Journal.* https://doi.org/10.30955/gnj.005279.
[26] Leema Margret, A., Karthikeyan, G., Ajandhadevi, S., Jenitha, G., Subalakshmi, M. 2023. Numerical Study on Flexural Behavior of Reinforced Concrete Beam Using MATLAB. *AIP Conference Proceedings.* 2831: 060004. https://doi.org/10.1063/5.0162709.
[27] Karthikeyan, G., Leema Margret, A., Muruganantham, R., Harshani, R. 2024. Influence of Utilizing Prosopis Juliflora Ash as Cement on Mechanical Properties of Cement Mortar and Concrete. *Global NEST Journal.*
[28] Karthikeyan, G., Leema Margret, A., Vineeth, V., Harshani, R. 2023. Expeimental Study on Mechanical Properties of Textile Reinforced Concrete. *E3s Web of Conferences.*
[29] Omar Sore *et al*. 2023. Effect of Portland Cement on Mechanical and Durability Properties of Geopolymer Concrete at Ambient Temperature. *Civil Engineering Journal*. 9(7).
[30] R. Balamuralikrishnan *et al*. 2023. Seismic Upgradation of RC Beams Strengthened with Externally Bonded Spent Catalyst Based Ferrocement Laminates. *HighTec and Innovation Journal.* 4(1).
[31] Al-Kasassbeh *et al*. 2023. Influential and Intellectual Structure of Geopolymer Concrete: A Bibliometric Review. *Civil Engineering Journal.* 9(9).